Paper No. 8

Advances in Experiment Design for High Performance Aircraft

Eugene A. Morelli

MS 132
NASA Langley Research Center
Hampton, VA 23681 - 0001

NATO Defense Research & Technology Organization

Symposium on System Identification for Integrated Aircraft Development and Flight Testing

May 5 - 7, 1998 / Madrid, Spain

ADVANCES IN EXPERIMENT DESIGN FOR HIGH PERFORMANCE AIRCRAFT

Eugene A. Morelli

Dynamics and Control Branch
MS 132, NASA Langley Research Center
Hampton, Virginia 23681 - 2199 USA

SUMMARY

A general overview and summary of recent advances in experiment design for high performance aircraft is presented, along with results from flight tests. General theoretical background is included, with some discussion of various approaches to maneuver design. Flight test examples from the F-18 High Alpha Research Vehicle (HARV) are used to illustrate applications of the theory. Input forms are compared using Cramér-Rao bounds for the standard errors of estimated model parameters. Directions for future research in experiment design for high performance aircraft are identified.

LIST OF SYMBOLS

a_y, a_z	linear accelerations, g's
$E\{\ \}$	expectation operator
J	cost function
L, M, N	body axis aerodynamic moments
$\boldsymbol{M}$	information matrix
N	total number of sample times
p, q, r	body axis angular velocities, rad/sec
$\boldsymbol{R}$	discrete noise covariance matrix
$S(i)$	output sensitivity matrix at time $i\Delta t$
T	maneuver duration, sec
$\boldsymbol{u}$	n_i-dimensional control vector
V	airspeed, ft/sec
$\boldsymbol{x}$	n_x-dimensional state vector
$\boldsymbol{y}$	n_o-dimensional output vector
$y(i)$	output vector at time $i\Delta t$
$z(i)$	measured output vector at time $i\Delta t$
Y, Z	body axis aerodynamic forces
α	angle of attack, rad
β	sideslip angle, rad
δ_{ij}	Kronecker delta
Δt	sampling interval, sec
δ_a	aileron deflection, rad
δ_r	rudder deflection, rad
δ_s	stabilator deflection, rad
ϕ, θ, ψ	Euler angles, rad
η_e	longitudinal stick deflection
η_a	lateral stick deflection
η_r	rudder pedal deflection
μ_j	jth input amplitude constraint
$\nu(i)$	ith discrete measurement noise vector
θ	n_p-dimensional parameter vector
θ_j	jth model parameter
σ_j	Cramér-Rao bound for the jth parameter
τ_a	lateral stick equivalent time delay, sec
τ_r	rudder pedal equivalent time delay, sec
ξ_k	kth output amplitude constraint
$\forall$	for all, for every
Tr	trace

Superscripts

T	transpose
-1	matrix inverse

Subscripts

o	average or trim value
s	stability axis

1. INTRODUCTION

Aircraft flight tests designed to collect data for modeling purposes are generally motivated by one or more of the following objectives:

1. The desire to correlate aircraft aerodynamic characteristics obtained from wind tunnel experiments and aerodynamic calculations with flight test data.
2. Refinement of the aircraft model for control system analysis and design.
3. Accurate prediction of the aircraft response using the mathematical model, including flight simulation and flight envelope expansion.
4. Aircraft acceptance testing.

The design of an experiment to achieve any of the above objectives involves specification of the instrumentation, the signal conditioning, the flight test operational procedure, the inputs for the flight test maneuver, the model structure, and the data analysis methods. In this work, the maneuver design – specifically, design of flight test input signals – will be studied independently of the other aspects which impact the success of the flight test.

The flight test maneuver (equivalently, the flight test input) has a major impact on the quality of the data for modeling purposes. Designing an input for accurate model parameter estimation requires rich excitation of the system, which is frequently at odds with various practical constraints. One such practical constraint is the requirement that output amplitude excursions (e.g., in angle of attack or sideslip angle) about the flight test condition be limited in order to assure the validity of an assumed model structure. Input amplitudes must be constrained for the same reasons, and to avoid nonlinearities such as mechanical stops and rate limiting when the model is linear. These practical constraints translate to amplitude constraints on the inputs and outputs during the flight test.

Tests for high performance aircraft often involve flight at high angles of attack, sometimes using drop models. In these cases, flight test time is extremely limited due to rapid altitude loss, and it is imperative that information content in the data per unit of flight time be maximized for effective use of expensive flight test time. Such considerations highlight the importance of optimizing the flight test inputs.

In general, an aircraft model contains multiple response variables, multiple aircraft model parameters, and one or more inputs. The overall goal is to design a maneuver that produces data from which model parameters can be estimated accurately. This translates into exciting the system modes so that the sensitivities of the model outputs to the parameters are high and correlations among these sensitivities are low. Frequency sweep inputs[1] can be used to do this, requiring little more than knowledge of the frequency range of interest for the modeling. This technique is restricted to moving a single input at a time, so that off-axis responses or coupled motions are generally not well modeled from frequency sweep data. Frequency sweeps also require relatively long maneuver times (i.e., 1-2 minutes) to run through the frequency range of interest. Low frequency components of the frequency sweep contribute to long maneuver times, and also increase the tendency for the aircraft to depart from the desired flight test condition. For high performance aircraft, limited flight test time, multiple control effectors, and flight conditions such as high angle of attack make the frequency sweep approach difficult to use and expensive.

An alternate approach is to take advantage of *a priori* knowledge about the dynamics of the aircraft to focus the input energy at frequencies near the system modes. An *a priori* model can be assembled using wind tunnel aerodynamic data and knowledge of rigid body dynamics and the control system. With the *a priori* model, a short flight test maneuver can be designed to produce data with high information content. Resulting flight test data can be analyzed using a variety of methods in the time and frequency domains. A paradox occurs here, in that very good inputs will be designed when the *a priori* model is very good; however, in this case the experiment is less needed. Obviously, the input design technique must be robust to errors in the *a priori* model.

Designing an input that excites the aircraft dynamic response as much as possible when modal frequencies are imperfectly known, while simultaneously satisfying practical constraints, is a difficult problem. Several researchers have studied the problem of finding optimal inputs for aircraft parameter estimation[2-11]. The most serious obstacles to using the results of these studies in flight have been practical implementation issues. These include unrealizable optimal input forms, and failure to account for closed-loop control, actuator dynamics, or constraints on input and output amplitudes. Computationally, the difficulties have been selection of an appropriate optimality criterion, inadequate numerical optimization techniques for finding global optimal solutions, and difficulties associated with multiple input design.

Recent research[12-16] has produced an optimal input design technique which addresses the above issues. The technique generates square wave inputs which are globally optimal in the sense that information content in the data is maximized for a fixed flight test time, or, alternatively, specified parameter accuracy goals are achieved in minimum flight test time.

The global optimal square wave input design technique has been shown to be theoretically sound[12,13], has been validated in flight for aerodynamic model parameter estimation experiments using pilot implementation, including demonstrated higher parameter accuracies compared to compound doublet inputs[14], has been used successfully to specify flight test maneuvers for closed loop model identification at high angles of attack[15], has shown improved parameter accuracy in comparison to doublet and 3-2-1-1 inputs in flight tests[16], and has compared favorably to other techniques in the literature for a standard test problem[17]. In Ref. [17], the global optimal square wave input produced the lowest value of the sum of estimated parameter variances, even though the maneuver time allotted for this design was the smallest of any of the techniques studied (see Table 3 of Ref. [17], p. 281). This fact, though not pointed out by the authors of Ref. [17], demonstrates the effectiveness of the global optimal square wave input design technique.

The purpose of this work is to give an overview of NASA research on optimal input design for high performance aircraft, and to present relevant flight test results. The next section outlines the theory involved in optimal input design, and discusses the choices made in developing the global optimal square wave input design technique. Next, the F-18 High Alpha Research Vehicle (HARV) test aircraft and some details of flight test procedure are described. Following this, results from selected flight tests are presented and discussed.

2. THEORETICAL DEVELOPMENT

Airplane dynamics can be described by the following linear model equations:

$$\dot{x}(t) = Ax(t) + Bu(t) \tag{1}$$

$$x(0) = x_o \tag{2}$$

$$y(t) = Cx(t) + Du(t) \tag{3}$$

$$z(i) = y(i) + v(i) \quad i = 1, 2, \ldots, N \tag{4}$$

Linear models are used in Eqs. (1) and (3) because of the common practice of estimating stability and control derivatives from flight test data collected at a chosen flight condition. Elements of the system matrices A, B, C, and D contain stability and control derivatives, which are the unknown model parameters to be estimated from flight test data. If the maneuver is designed for small perturbations of the inputs and outputs about a chosen flight condition, the stability and control derivatives can be assumed constant. Measurement noise $v(i)$ is assumed Gaussian with

$$E\{v(i)\} = 0 \quad \text{and} \quad E\left\{v(i)v(j)^T\right\} = R\delta_{ij} \tag{5}$$

Eqs. (1)-(5) can be used to characterize bare airframe dynamics, where the inputs are control surface deflections and the outputs can include air data (V, α, β), body axis angular velocities (p, q, r), Euler angles (ϕ, θ, ψ), and translational accelerations (a_x, a_y, a_z). The same general model structure can be used to characterize closed loop dynamics, where the inputs are pilot stick and rudder deflections and the outputs are selected from the same list as before. For closed loop modeling, the input includes a pure time delay τ, called the equivalent time delay, to account for phase lag effects from sources such as high order control system dynamics, digital sampling delay, and actuator dynamics. For either bare airframe or closed loop modeling, longitudinal and lateral cases are treated separately, with the linear model structure shown above resulting from the usual small perturbation assumptions.

Constraints arising from practical flight test considerations can be represented as limits on all input amplitudes and selected output amplitudes. Input amplitudes are limited by mechanical stops, flight control software limiters, rate limits, or linear control effectiveness. Selected output amplitudes must be limited to avoid departure from the desired flight test condition and to ensure validity of the assumed linear model structure. In addition, constraints may be required on aircraft attitude angles for flight test operational considerations, such as flight safety and maintaining line of sight from the downlink antenna aboard the aircraft to the ground station. These constraints are specified by

$$|u_j(t)| \le \mu_j \quad \forall t \qquad j = 1, 2, \ldots, n_i \tag{6}$$

$$|y_k(t)| \le \xi_k \quad \forall t \qquad k \in (1, 2, \ldots, n_o) \tag{7}$$

where μ_j and ξ_k are positive constants.

Some researchers have implemented practical flight test constraints using an energy constraint on the input,

$$\int_0^T u(t)^T u(t)\, dt = E \tag{8}$$

where E is some fixed value of the allowable input energy, chosen by experience or intuition. This constraint is intended to limit input and output amplitudes, but it is also chosen for convenience in the optimization. Input energy is typically introduced as a constraint on the input form, while the cost function quantifying achievable model parameter accuracy based on the data is optimized using variational calculus to arrive at an optimal input design. In practice, there is no direct constraint on the amount of input energy which can be applied during the flight test, since neither the pilot nor the control system have inherent energy limitations. The practical flight test situation dictates that the constraints be directly on the amplitudes of both the input and the output variables, as given by Eqs. (6) and (7), respectively. The constraint in Eq. (8) limits the input and output amplitudes indirectly with an integral expression.

When estimating model parameter values from measured data, the minimum achievable parameter standard errors using an asymptotically unbiased and efficient estimator (such as maximum likelihood) are called the Cramér-Rao lower bounds[12,18,19]. The Cramér-Rao lower bounds for the parameter standard errors are computed as the square root of the diagonal elements of the dispersion matrix $\mathcal{D}$[12,18,19]. The dispersion matrix is defined as the inverse of the information matrix M, the latter being a measure of the information content of the data from an experiment. The expressions for these matrices are

$$M = \sum_{i=1}^{N} S(i)^T R^{-1} S(i) \tag{9}$$

$$\mathcal{D} = M^{-1} \tag{10}$$

where $S(i)$ is the matrix of output sensitivities to the parameters,

$$S(i) = \left.\frac{\partial y(i)}{\partial \theta}\right|_{\theta=\hat{\theta}} \tag{11}$$

and $\hat{\theta}$ denotes the parameter vector estimate.

The information matrix can be loosely interpreted as signal-to-noise ratio for multiple output, multiple parameter linear systems. In this interpretation, the signal is the sensitivity of the outputs to the parameters. If these sensitivities are large relative to the noise level (3 to 1 ratio or greater) and are

uncorrelated with one another, then the output dependence on the parameters is strong and distinct for each parameter. Parameter values can then be estimated with high accuracy when adjusting each of the parameters so that model outputs match measured outputs in a least squares sense. Elements of the information matrix also depend on the measurement sampling rate and the measurement noise characteristics, which are determined when specifying the instrumentation system.

The output sensitivities for the jth parameter appear as the jth column of the sensitivity matrix, and are computed from

$$\frac{d}{dt}\left[\frac{\partial \boldsymbol{x}}{\partial \theta_j}\right] = \boldsymbol{A}\frac{\partial \boldsymbol{x}}{\partial \theta_j} + \frac{\partial \boldsymbol{A}}{\partial \theta_j}\boldsymbol{x} + \frac{\partial \boldsymbol{B}}{\partial \theta_j}\boldsymbol{u} \qquad (12)$$

$$\frac{\partial \boldsymbol{x}}{\partial \theta_j}(0) = \boldsymbol{0} \qquad (13)$$

$$\frac{\partial \boldsymbol{y}}{\partial \theta_j} = \boldsymbol{C}\frac{\partial \boldsymbol{x}}{\partial \theta_j} + \frac{\partial \boldsymbol{C}}{\partial \theta_j}\boldsymbol{x} + \frac{\partial \boldsymbol{D}}{\partial \theta_j}\boldsymbol{u} \qquad (14)$$

for $j = 1, 2, \ldots, n_p$. Eqs. (12)-(14) follow from differentiating Eqs. (1)-(3) with respect to θ_j, combined with the assumed analyticity of $\boldsymbol{x}$ in the model equations. Note that it is necessary to have nominal (*a priori*) values for the model parameters to solve Eqs. (12)-(14). The output sensitivities $S(i)$ can also be computed using finite difference perturbations from the nominal parameter values and Eqs. (1)-(3).

From Eqs. (9)-(14), it is clear that the information matrix elements (and therefore the Cramér-Rao bounds) depend on the input through the sensitivity equations (12)-(14). The input $\boldsymbol{u}$ influences the sensitivities both directly as a forcing function in the sensitivity equations and indirectly as an influence on the states, which also force the sensitivity equations. The dependence of the Cramér-Rao bounds on the input is nonlinear in the input amplitude, regardless of whether or not the system equations (1) and (3) are linear, because of the nonlinear character of Eqs. (9) and (10).

Eq. (9) is a discrete approximation to a time integral over the maneuver duration $T = N\Delta t$. Therefore, when comparing the effectiveness of various input designs using some function of the dispersion matrix $\mathcal{D}$ as the criterion for comparison, the input designs being compared should have the same maneuver duration, and in light of the last paragraph, also the same allowable maximum input amplitude. This approach contrasts with comparisons presented in previous works[9,10,11,17], which were based on constant input energy. If only constant input energy is imposed on all inputs, a comparison among the inputs using a criterion which is a function of $\mathcal{D}$ is inherently unfair because a wide range of values for maximum allowable input amplitude and maneuver duration can give the same input energy.

Similarly, the dispersion matrix $\mathcal{D}$ depends nonlinearly on the states, which are often the same as the outputs. Therefore, output amplitudes must be comparable if an input design comparison is to be focused only on the merits of the input forms. For this reason, as well as to ensure validity of the assumed model structure, the inputs should be designed to produce comparable output amplitudes. If the maneuver duration, input amplitudes, and output amplitudes are not the same for all input designs being compared, it is possible to arrange matters so that almost any chosen input form will appear to be the best, based on a criterion function that depends on $\mathcal{D}$.

For the global optimal square wave input design, the flight test maneuver duration $T = N\Delta t$ might be fixed *a priori* due to practical time constraints of the flight test or an analysis of the rate of decrease of the Cramér-Rao bounds with increasing maneuver time using the optimized input. For the flight test examples included in this work, the cost function to be minimized for a fixed maneuver duration was the sum of squares of the Cramér-Rao bounds for the parameter standard errors,

$$J = \sum_{j=1}^{n_p} \sigma_j^2 = Tr\left[\boldsymbol{M}^{-1}\right] = Tr[\mathcal{D}] \quad \text{for a given } T \qquad (15)$$

Another formulation of the cost can be defined to design the input for minimum flight test time to achieve specific goals for the Cramér-Rao bounds[12]. This is a minimum time problem, so that the cost is given by

$$J = T \quad \text{when } \sigma_k \le \xi_k \quad \forall k = 1, 2, \ldots, n_p \qquad (16)$$

For the flight test examples included here, the optimal input applied to the dynamic system described by Eqs. (1)-(5) minimized the cost function in Eq. (15), subject to the constraints in Eqs. (6) and (7).

3. OPTIMAL INPUT SOLUTION

The optimization problem posed in the last section is difficult to solve in general. For the particular problem of optimal input design for aircraft parameter estimation, there are good reasons to restrict the allowable input form to full amplitude square waves only. Among these are analytical work on a similar problem[6], which indicated that the optimal input should be "bang-bang" (i.e., a full amplitude switching input). Square wave inputs are simple to implement for either an onboard computer or the pilot. Finally, several flight test evaluations[10,14,16,17] have demonstrated that square wave inputs were superior to sinusoidal and doublet inputs for parameter estimation experiments, largely due to richer frequency spectra.

For the above reasons, and to make the optimization problem tractable, input forms were limited to full amplitude square waves only; i.e., only full positive, full negative, or zero amplitude was allowed for any input at any time. Full input amplitude was used in

order to excite the system as much as possible. Choice of the pulse timing and having zero amplitude available gave the optimizer the ability to use full input amplitudes without exceeding output amplitude constraints. With the above restrictions on the input form, the problem becomes a high order combinatorial problem involving output amplitude constraints, which is well-suited to solution by the method of dynamic programming.

Dynamic programming is essentially a very efficient method for doing a global exhaustive search. Arbitrary dynamics such as control surface actuator dynamics, feedback control, and general nonlinear models can therefore be included inside the optimization without difficulty. The result obtained is a globally optimal square wave input obtained in a single pass solution. The technique includes provisions to adjust the input possibilities at certain times in order to account for practical limitations on frequency content of the input, such as avoiding structural resonance frequencies. The dynamic programming solution smoothly handles the multiple input problem, since this just changes the number of square wave input possibilities. Keeping the system responses within the output space for which the assumed model structure is valid can be handled directly with dynamic programming by discarding any input sequence whose output trajectory exceeds the constraint limits. More details on the dynamic programming solution method can be found in Refs. [12] and [13].

4. AIRCRAFT AND TEST PROCEDURES

The F-18 High Alpha Research Vehicle (HARV) is a modified F/A-18 fighter[20]. The flight test inputs were implemented by the pilot, and also by a computer-controlled On-Board Excitation System (OBES).

The pilot initiated each maneuver by first trimming the aircraft at the specified flight condition. For the piloted square wave inputs, the pilot signaled the ground controllers to send the square wave input sequence via the uplink from a computer on the ground. The maneuver was described by required stick and rudder deflections, represented to the pilot as movements of a cockpit indicator in real time. Accurate implementation of the input was achieved if the pilot accurately tracked the indicator movement with his own stick and rudder inputs. Using this procedure, the pilot was able to produce a high fidelity realization of the desired square wave inputs.

For square wave inputs implemented by the OBES, the pilot first selected a pre-programmed maneuver using buttons on a Digital Display Interface (DDI) inside the cockpit. The aircraft was then brought to the desired trimmed flight condition and an engage/disengage button on the DDI was pressed to initiate the maneuver. Square wave perturbation inputs from the OBES were added directly to the appropriate control surface actuator commands (for bare airframe modeling) or to pilot stick and rudder commands (for closed loop modeling), with the feedback control system still operating. The pilot held stick and rudder deflections constant at the trimmed values until the maneuver was complete. The maneuver could be disengaged manually by the pilot toggling the engage/disengage button, or automatically by the research flight control system, based on g-limits, etc. The pre-programmed square wave perturbation inputs were standard 3-2-1-1 inputs, doublets, or square waves obtained from the optimal input design technique described above.

Various downlink data transmission rates were employed on the F-18 HARV aircraft, but all of the data used for analysis was converted to a common sampling rate of 40 Hz. Corrections were applied to the angle of attack, sideslip angle, and linear accelerometer measurements to account for sensor offsets from the center of gravity, and the angle of attack measurement was corrected for upwash. Data compatibility analysis[21] revealed the need for a scale factor correction on the angle of attack and sideslip angle measurements from the wing tip vane, and small bias error corrections on the measurements from the rate gyros and accelerometers.

5. FLIGHT TEST RESULTS

For bare airframe short period longitudinal dynamics, the state vector $\boldsymbol{x}$, input vector $\boldsymbol{u}$, and output vector $\boldsymbol{y}$ in Eqs. (1)-(4) are defined by

$$\boldsymbol{x}=[\alpha \quad q]^T \quad \boldsymbol{u}=[\delta_s \quad 1]^T \quad \boldsymbol{y}=[\alpha \quad q \quad a_z]^T \tag{17}$$

System matrices containing the model parameters are:

$$\boldsymbol{A}=\begin{bmatrix} Z_\alpha & 1+Z_q \\ M_\alpha & M_q \end{bmatrix} \quad \boldsymbol{B}=\begin{bmatrix} Z_{\delta_s} & Z_o \\ M_{\delta_s} & M_o \end{bmatrix} \tag{18}$$

$$\boldsymbol{C}=\begin{bmatrix} 1 & 0 \\ 0 & 1 \\ \frac{V_o}{g}Z_\alpha & \frac{V_o}{g}Z_q \end{bmatrix} \quad \boldsymbol{D}=\begin{bmatrix} 0 & 0 \\ 0 & 0 \\ \frac{V_o}{g}Z_{\delta_s} & a_{z_o} \end{bmatrix} \tag{19}$$

For bare airframe lateral-directional dynamics,

$$\boldsymbol{x}=[\beta \quad p \quad r \quad \phi]^T \quad \boldsymbol{u}=[\delta_r \quad \delta_a \quad 1]^T \tag{20}$$

$$\boldsymbol{y}=[\beta \quad p \quad r \quad \phi \quad a_y]^T \tag{21}$$

System matrices $\boldsymbol{A}$, $\boldsymbol{B}$, $\boldsymbol{C}$, and $\boldsymbol{D}$ contain the model parameters:

$$\boldsymbol{A}=\begin{bmatrix} Y_\beta & Y_p+\sin\alpha_o & Y_r-\cos\alpha_o & \frac{g}{V_o}\cos\Theta_o \\ L_\beta & L_p & L_r & 0 \\ N_\beta & N_p & N_r & 0 \\ 0 & 1 & \tan\Theta_o & 0 \end{bmatrix} \tag{22}$$

$$\boldsymbol{B}=\begin{bmatrix} Y_{\delta_r} & Y_{\delta_a} & Y_o \\ L_{\delta_r} & L_{\delta_a} & L_o \\ N_{\delta_r} & N_{\delta_a} & N_o \\ 0 & 0 & \dot{\phi}_o \end{bmatrix} \tag{23}$$

$$\boldsymbol{C}=\begin{bmatrix} 1 & 0 & 0 & 0 \\ 0 & 1 & 0 & 0 \\ 0 & 0 & 1 & 0 \\ 0 & 0 & 0 & 1 \\ \frac{V_o}{g}Y_\beta & 0 & 0 & 0 \end{bmatrix} \tag{24}$$

$$\boldsymbol{D}=\begin{bmatrix} 0 & 0 & 0 \\ 0 & 0 & 0 \\ 0 & 0 & 0 \\ 0 & 0 & 0 \\ \frac{V_o}{g}Y_{\delta_r} & \frac{V_o}{g}Y_{\delta_a} & a_{y_o} \end{bmatrix} \tag{25}$$

For closed loop lateral-directional dynamics in stability axes, the model is

$$x=\begin{bmatrix}\beta & p_s & r_s & \phi\end{bmatrix}^T \tag{26a}$$

$$u=\begin{bmatrix}\eta_r(t-\tau) & \eta_a(t-\tau) & 1\end{bmatrix}^T \tag{26b}$$

$$y=\begin{bmatrix}\beta & p_s & r_s & \phi & a_y\end{bmatrix}^T \tag{27}$$

$$\boldsymbol{A}=\begin{bmatrix} Y_\beta & Y_p & Y_r-1 & \frac{g}{V_o}\cos\Theta_o \\ L_\beta & L_p & L_r & L_\phi \\ N_\beta & N_p & N_r & N_\phi \\ 0 & \frac{\cos\Gamma_o}{\cos\Theta_o} & \frac{\sin\Gamma_o}{\cos\Theta_o} & 0 \end{bmatrix} \tag{28}$$

$$\boldsymbol{B}=\begin{bmatrix} Y_{\eta_r} & Y_{\eta_a} & Y_o \\ L_{\eta_r} & L_{\eta_a} & L_o \\ N_{\eta_r} & N_{\eta_a} & N_o \\ 0 & 0 & \dot{\phi}_o \end{bmatrix} \tag{29}$$

$$\boldsymbol{C}=\begin{bmatrix} 1 & 0 & 0 & 0 \\ 0 & 1 & 0 & 0 \\ 0 & 0 & 1 & 0 \\ 0 & 0 & 0 & 1 \\ \frac{V_o}{g}Y_\beta & \frac{V_o}{g}Y_p & \frac{V_o}{g}Y_r & 0 \end{bmatrix} \tag{30}$$

$$\boldsymbol{D}=\begin{bmatrix} 0 & 0 & 0 \\ 0 & 0 & 0 \\ 0 & 0 & 0 \\ 0 & 0 & 0 \\ \frac{V_o}{g}Y_{\eta_r} & \frac{V_o}{g}Y_{\eta_a} & a_{y_o} \end{bmatrix} \tag{31}$$

The L_ϕ and N_ϕ terms are present in the closed loop lateral-directional model equations because the control law used bank angle feedback for gravity compensation to coordinate stability axis rolls. Closed loop model parameters are in general different from the bare airframe parameters, because the closed loop model parameters include the dynamics of the control system in addition to the bare airframe. Model equations could also be written using non-dimensional parameters[18].

A priori linear models used for the input design cases included here were derived from a nonlinear batch simulation of the F-18 HARV[22], which uses a wind tunnel database for the aerodynamics. Noise variance estimates for the *a priori* models were obtained from previous flight test data records using an optimal Fourier smoothing technique[23]. The models used for parameter estimation from flight test data were identical in structure to the *a priori* models, except that the *a priori* models did not include linear accelerometer outputs.

All flight test data analysis was done using output error maximum likelihood parameter estimation[18,19,24]. For the closed loop modeling, the equivalent time delays were estimated as the pure time delay from pilot input to control surface deflection. The equivalent time delay can be estimated very accurately this way because the signals involved have very low noise levels and the pilot inputs were square waves. Equivalent time delay was then held fixed at this estimated value during the maximum likelihood estimation. The Cramér-Rao bounds for the parameter standard errors were the square root of the diagonal elements of the dispersion matrix $\mathcal{D}$ computed from Eq. (10). In the time domain, a correction for colored output residuals from maximum likelihood estimation is necessary if the Cramér-Rao bounds are to accurately represent the error in the parameter

estimates[19,25]. The correction was not applied to the time domain results given here, because the input comparison results were unaffected by it, and also because the Cramér-Rao bounds used in the optimal input design assumed white Gaussian measurement noise. The same white noise assumption is made in computing the Cramér-Rao bounds from flight test data using output error maximum likelihood estimation. For flight test data analysis in the frequency domain, the correction is not necessary. Refs. [19] and [25] address this issue in detail. Model structure was held constant for the compared maneuvers, so that the number of parameters estimated from each data record was identical. All data analysis and parameter estimation was done using angle measurements in radians, but the plots were made using degrees.

The first input design was a bare airframe lateral-directional case using the OBES to implement sequential rudder and aileron inputs. The flight condition was 5 deg angle of attack, Mach 0.6, and altitude of approximately 25,000 ft. The model was given by Eqs. (1)-(5) and (20)-(25). Perturbation input and output amplitude constraints resulting from various practical flight test constraints were:

$$|\delta_r| \le 4.0 \text{ deg} \qquad |\delta_a| \le 2.5 \text{ deg} \qquad (32a)$$

$$|\beta| \le 5.0 \text{ deg} \qquad |\phi| \le 32.0 \text{ deg} \qquad (32b)$$

The 3-2-1-1 input form has been shown to be very effective for aircraft parameter estimation in previous flight test investigations[9,10], so this input was chosen to compare with the globally optimal square wave input design. Standard 3-2-1-1 inputs and globally optimal square wave inputs were designed using the same input amplitude constraints in (32a), the same maneuver duration, the same *a priori* model, and the same output amplitude constraints in (32b).

The 3-2-1-1 inputs were designed by matching the frequency of the "2" pulse to the frequency of the dominant oscillatory mode for the *a priori* model, and adjusting amplitudes and control sequence timing so that the chosen output amplitude constraints were satisfied. Optimal inputs were designed with a computer program that implemented the optimal input design procedure described above[12]. The duration of each maneuver was 24 seconds.

Figures 1 and 2 show the input and output time histories measured in flight for the OBES lateral-directional 3-2-1-1 and optimal inputs at 5 degrees angle of attack. The solid lines on the left side of Figures 1 and 2 are the commanded inputs from the OBES, and the dashed lines are the actual measured control surface positions. The desired input forms were distorted by the feedback control system, as can be seen in the figures. The distortion of the input forms by the lateral-directional feedback control system was not accounted for in the design process for either input design. Figures 1 and 2 show that the maximum input and output amplitudes for these two maneuvers were very nearly the same, and the length of each maneuver was the same. The maneuvers were run in immediate succession on the same flight. With the model structure held fixed for the data analysis on each maneuver, any differences in the resulting model parameter accuracies can be attributed to effect of the input form.

Parameter estimation results for the OBES lateral-directional 3-2-1-1 and optimal inputs at 5 degrees angle of attack are given in Table 1. Column 1 in Table 1 lists the model parameters, column 2 contains the *a priori* values of the parameters used for the input design, column 3 contains parameter estimates and Cramér-Rao lower bounds for the parameter standard errors using the 3-2-1-1 input. Column 4 contains the corresponding results for the optimal square wave input. The dashed lines on the right side of Figures 1 and 2 are the model responses computed using the measured inputs and the estimated model parameters from columns 3 and 4 of Table 1. The match is very good in both cases.

Values in column 5 of Table 1 are the percent change in the Cramér-Rao bound for each model parameter standard error for the optimal input maneuver compared to the 3-2-1-1 maneuver, based on the 3-2-1-1 value. The optimal input reduced parameter standard errors (equivalently, increased parameter accuracy) by an average 20%, with lower parameter standard errors for every estimated parameter. Parameter estimates in columns 3 and 4 of Table 1 are generally in good agreement.

The percent error of the *a priori* parameter values relative to the parameter values estimated from flight test data (computed as the average of values in columns 3 and 4 of Table 1) varied from 4.2% to 65.1%, with an average value of 24.2%. Nevertheless, both input design methods based on the *a priori* model produced experimental data with excellent information content, as evidenced by the low standard error bounds in Table 1.

Symmetric stabilator input designs implemented by OBES for longitudinal model identification are shown in Figures 3 and 4. In this case, the distortion of the input forms by the feedback control was accounted for in the *a priori* model by including a linear model of the feedback control identified from the nonlinear simulation. The same *a priori* design model was used to design both inputs shown in Figures 3 and 4. The flight condition was again 5 deg angle of attack, Mach 0.6, and altitude of approximately 25,000 ft. The model used for the parameter estimation is given by Eqs. (1)-(5) and (17)-(19). The same methods were used for the input designs and the data analysis, except that the optimal input design was allowed a higher input amplitude than the 3-2-1-1 input. This was done to investigate the capability available with the optimal input design routine to use higher input amplitudes for increased parameter accuracies while maintaining the same output amplitude constraints. Such flexibility is not available with the 3-2-1-1 input because of its fixed form. Perturbation input and output amplitude constraints were:

$$|\delta_s| \le 3.0 \text{ deg} \quad \text{for the 3-2-1-1 input}$$
$$|\delta_s| \le 4.0 \text{ deg} \quad \text{for the optimal input} \qquad (33a)$$

$$|\alpha| \le 3.0 \text{ deg} \qquad (33b)$$

Each maneuver lasted 26 seconds, and the maneuvers were run in immediate succession on the same flight. The left sides of Figures 3 and 4 show the significant distortion of the stabilator commands resulting from the longitudinal feedback control. Parameter estimation results are given in Table 2 using the same format as Table 1. The parameter accuracies are now improved by an average 72% using the optimal input compared to the 3-2-1-1 input. The optimal input maneuver produced larger α perturbations than the 3-2-1-1, although maximum α amplitude was the same for both inputs in the design phase using the *a priori* model. The reason for this discrepancy was that the control law removed most of the "3" pulse for the 3-2-1-1, and this effect was not well modeled in the *a priori* model. The optimal input used shorter pulses in general, and thus was less affected. The dashed lines on the right sides of Figures 3 and 4 indicate a good match between the measured outputs and the model responses using the measured inputs and the estimated model parameters from columns 3 and 4 of Table 2. The estimates of pitching moment parameters in columns 3 and 4 of Table 2 do not agree. Lower parameter standard error bounds for the optimal input indicate that the pitching moment parameter estimates from the optimal input should be more accurate. To check this, a different maneuver at the same flight condition was used to investigate the prediction capability of the models using the parameters in Table 2. Figure 5 shows measured and predicted pitch rate response using the model parameters from Table 2 with the same model structure used before. The stabilator input (not shown) was a perturbation input with amplitude approximately ±5 deg from the trim value of 2 deg. The stabilator input was applied to both models to produce the prediction responses plotted with the measured response in Figure 5. The prediction using the parameters estimated from the 3-2-1-1 input (shown on the left side of Figure 5) was less accurate than the prediction using the parameters from the optimal input (shown on the right side of Figure 5), both in frequency and amplitude. This result gives confidence that the parameters estimated from the optimal input maneuver are indeed more accurate, as indicated by the computed Cramér-Rao bounds.

Next, two longitudinal maneuvers flown at 20 deg angle of attack, Mach 0.4, and approximately 25,000 feet altitude are studied to compare the optimal square wave input design to a sequence of doublets. The maneuvers were implemented by the pilot in this case, using the procedure described in section 4 above. The objective was accurate modeling of the bare airframe short period dynamics. Perturbation input and output amplitude constraints were:

$$|\eta_e| \le 1.0 \text{ in} \qquad (34a)$$

$$|\alpha| \le 4.5 \text{ deg} \qquad (34b)$$

Each maneuver lasted 14 seconds. The left side of Figure 6 shows the pilot longitudinal stick deflection for the doublet sequence. The right side of Figure 6 shows the target optimal square wave input (dashed line) with the pilot's realization of that target input in flight (solid line). The pilot's realization of the optimal square wave input is highly accurate in frequency, but somewhat inaccurate in amplitude. The inputs shown in Figure 6 have similar maximum input amplitudes. Table 3 contains the results of maximum likelihood parameter estimation using the same longitudinal model structure as before. Compared to the doublet sequence input, the optimal square wave input maneuver produced lower parameter standard errors (higher accuracy) for every model parameter, despite distortion in the pilot's implementation of the optimal square wave input. The average improvement was 47%, based on the standard error value from the doublet sequence maneuver. This example demonstrates that the optimal square wave input design is robust to distortion, and can be successfully implemented by a pilot in flight.

The next optimal input design example is a closed loop modeling case executed using the OBES at 60 deg angle of attack, Mach 0.25, and average altitude approximately 24,000 ft. At this high angle of attack, the aircraft sink rate was approximately 150 feet per second, as altitude dropped from 25,500 feet to 21,900 feet during the 24 second maneuver. Perturbation input and output amplitude constraints imposed for the input design were:

$$|\eta_r| \le 80 \text{ lbf} \qquad |\eta_a| \le 2.5 \text{ in} \qquad (35a)$$

$$|\beta| \le 5.0 \text{ deg} \qquad |\phi| \le 20.0 \text{ deg} \qquad (35b)$$

The solid lines in Figure 7 show the measured input and output time histories from flight for the lateral-directional optimal square wave inputs at 60 deg angle of attack. Since the square wave perturbation inputs were implemented by the OBES, the inputs realized in flight matched desired optimal inputs exactly; therefore, only one trace is shown for each input on the left side of Figure 7.

The data analysis was done using output error maximum likelihood parameter estimation in the frequency domain[24]. The model used for the parameter estimation is given by Eqs. (1)-(5) and (26)-(31).

Results for the OBES lateral-directional optimal inputs at 60 degrees angle of attack are given in Table 4. Column 1 in Table 4 lists the closed loop parameters, column 2 contains the *a priori* parameter values, and column 3 shows the parameter values estimated from flight test data. Column 4 contains the Cramér-Rao lower bounds for the parameter standard errors using flight test data from the optimal

square wave input maneuver. The dashed lines on the right side of Figure 7 indicate the model responses using the estimated closed loop model parameters from column 3 of Table 4 and the measured inputs. The match is good considering that the aerodynamic dependencies are generally nonlinear at this flight condition. The input and output amplitude constraints imposed during the input optimization restrained these nonlinearities throughout the maneuver, so that the assumed linear model structure could be used.

Comparing columns 2 and 3 of Table 4, the *a priori* model parameters were significantly different from the parameter values estimated from the flight test data. The percent error of the *a priori* parameter values relative to the parameters estimated from flight test data varied from 3.1% to 226.5%, with an average value of 41.9%. Nevertheless, the optimal input design based on the *a priori* model produced experimental data with excellent information content, as evidenced by the low standard error bounds in column 4 of Table 4. All pairwise correlations between estimated parameters were less than 0.8, with most below 0.2. This example demonstrates the robustness of the optimal input design technique to errors in the *a priori* model, as well as the applicability of the technique to closed loop flight test maneuver design at high angles of attack.

Figure 8 shows a prediction case at roughly the same flight condition as the last maneuver. The solid lines in Figure 8 represent measured flight test data. The dashed lines in Figure 8 were generated using the measured flight test inputs in Figure 8 and the closed loop model estimated from the flight test data of Figure 7 (i.e., model parameters from column 3 of Table 4). The plots in Figure 8 show the excellent prediction capability of the closed loop model estimated from flight test data generated by the optimal square wave inputs. This result gives confidence that the linear model can be usefully employed at high angles of attack, and moreover that such models can be accurately estimated from short data records using optimized square wave inputs.

Figure 9 shows flight test data for a lateral-directional optimal square wave input design implemented by the pilot. The maneuver was flown at 30 deg angle of attack, Mach 0.28, and average altitude of approximately 24,000 ft. The inputs were optimized with the square wave pulses constrained to be integer multiples of 0.5 second, and including a constraint that one second of zero input separate the rudder pedal and lateral stick input square waves (see Figure 9). These constraints were included to help the pilot accurately realize the optimal input form using the rudder pedals and the lateral stick in sequence. Such constraints can be easily incorporated into the dynamic programming optimization for the optimal square wave input design. Ref. [12] describes this feature of the optimal input design technique in detail. Perturbation input and output amplitude constraints imposed for the piloted optimal input design were:

$$|\eta_r| \le 102 \text{ lbf} \qquad |\eta_a| \le 1.5 \text{ in} \tag{36a}$$

$$|\beta| \le 6.0 \text{ deg} \qquad |\phi| \le 20.0 \text{ deg} \tag{36b}$$

Table 5 contains the maximum likelihood estimation results for the piloted optimal input, obtained in the same manner and presented in the same format as before for the OBES closed loop optimal input maneuver. The dashed lines on the left side of Figure 9 show the target optimal input, and the solid lines indicate the pilot's implementation in flight. The pilot inputs are again highly accurate in frequency (i.e., the square wave switching times were reproduced well), with some error in the amplitudes. The dashed lines on the right side of Figure 9 are the model responses using estimated closed loop model parameters from column 3 of Table 5 and the measured pilot inputs. As in the OBES closed loop optimal input case, the match is good despite higher order dynamics and nonlinearities in the physical system. The high accuracy of the estimated parameters shown in column 4 of Table 5 indicates that the optimal input design technique is robust to errors both in the *a priori* model, and in the implementation of the optimal square wave input form.

The parameter standard errors for this 30° α pilot implementation case were lower that those seen for the computer-implemented optimal input at 60° α, mainly due to the severe amplitude distortion by the pilot. If the distortion in the implementation of the optimal input (by the pilot or the feedback control system) can be characterized by linear dynamics (an excellent assumption in the case of the feedback control system distortion), then the effect of the input distortion on the flight test results is similar to the effect of errors in the *a priori* design model.

6. CONCLUDING REMARKS

The expense associated with flight testing high performance aircraft dictates that flight test data for modeling purposes be collected as efficiently as possible. This work reviewed some recent research in maneuver design for high performance aircraft, including examples from F-18 HARV flight tests.

Single and multiple input design cases were studied for bare airframe and closed loop modeling over a range of angles of attack, including fair comparisons of global optimal square wave inputs to conventional 3-2-1-1 and doublet input forms. The impact of the different input forms on estimated parameter accuracy was quantified through these investigations. For a flight test comparison done on an equal basis, the optimal square wave input decreased estimated parameter standard errors (equivalently, increased estimated parameter accuracy) by an average 20% compared to the 3-2-1-1 input. The decrease in estimated parameter standard errors improved to an average 72% using higher input amplitudes in the optimal input design while maintaining flight condition. Compared to a compound doublet sequence, the optimal input

decreased estimated parameter standard errors by an average 47% in a piloted flight test. For all the comparisons, every individual parameter was estimated more accurately using the optimal square wave input. These results were obtained with optimal square wave inputs implemented successfully by both the pilot and an onboard computer system.

The results of this investigation indicate that a properly designed 3-2-1-1 input can give good performance relative to the optimal square wave. Optimal square wave input designs demonstrated increased data information content in all cases studied, but the optimal input design technique is perhaps most valuable because of its ability to address practical design issues. Examples include an automated ability to limit output amplitude excursions during the flight test maneuver, good robustness to errors in the *a priori* model and to distortions in the realized input form, and the design flexibility to investigate the impact of changes in the conditions or constraints of the input design, such as available maneuver time, control surface rate limits, or input/output amplitude constraints. Such changes can be evaluated in terms of estimated parameter accuracies, using the single pass global optimizer in the optimal input design procedure. Some of these capabilities were demonstrated in this work using flight test results.

In the future, optimal design of maneuvers to collect data for dynamic modeling purposes should move off the engineer's workstation and onto the aircraft. This is possible because of increasing capabilities of flight control computers and improved understanding of the important aspects of the input optimization. Initial studies in this area are already underway[26]. In addition, research in the area of optimal input design for model parameter estimation should influence real time parameter estimation schemes that are required for adaptive and reconfigurable control. More areas to explore include optimal input design for nonlinear models, unsteady aerodynamic effects, and structural dynamics.

7. ACKNOWLEDGMENTS

Discussions with Dr. Vladislav Klein of the George Washington University contributed to the work presented here. Flight tests were carried out at NASA Dryden Flight Research Center, with Ed Schneider as pilot.

8. REFERENCES

1. Williams, J.N., Ham, J.A., and Tischler, M.B., "Flight Test Manual, Rotorcraft Frequency Domain Flight Testing", U.S. Army Aviation Technical Test Center, Edwards AFB, CA, AQTD Project No. 93–14, September 1995.
2. Stepner, D.E. and Mehra, R.K., "Maximum Likelihood Identification and Optimal Input Design for Identifying Aircraft Stability and Control Derivatives", NASA CR-2200, March 1973.
3. Mehra, R. K., "Optimal Input Signals for Parameter Estimation in Dynamic Systems - Survey and New Results", IEEE Transactions on Automatic Control, *AC-19*, 6, December 1974, pp.753-68.
4. Gupta, N.K. and Hall, W.E., Jr., "Input Design for Identification of Aircraft Stability and Control Derivatives", NASA CR-2493, February 1975.
5. Mehra, R. K. and Gupta, N. K., "Status of Input Design for Aircraft Parameter Identification", AGARD-CP-172, May 1975, paper 12.
6. Chen, R. T. N., "Input Design for Aircraft Parameter Identification: Using Time-Optimal Control Formulation", AGARD-CP-172, May 1975 paper 13.
7. Gupta, N.K. and Hall, W.E., Jr., "Model Structure Determination and Test Input Selection for Identification of Nonlinear Regimes", Office of Naval Research, Arlington, VA, Report ONR-CR215-213-5, February 1976.
8. Gupta, N.K., Mehra, R.K. and Hall, W.E., Jr., "Application of Optimal Input Synthesis to Aircraft Parameter Identification", Journal of Dynamic Systems, Measurement and Control, *98*, 2, June 1976, pp. 139-45.
9. Plaetschke, E. and Schulz, G., "Practical Input Signal Design", AGARD-LS-104, November 1979, paper 3.
10. Plaetschke, E., Mulder, J.A., and Breeman, J.H., "Flight Test Results of Five Input Signals for Aircraft Parameter Identification", *in* Proceedings of the Sixth IFAC Symposium on Identification and System Parameter Estimation, Pergamon Press, Vol. 2, June 1982, pp. 1149-1154.
11. Mulder, J. A., Sridhar, J.K., and Breeman, J.H., "Identification of Dynamic Systems – Applications to Aircraft, Part 2: Nonlinear Analysis and Manoeuvre Design", AGARD-AG-300, Vol. 3, Part 2, May 1994.
12. Morelli, E. A., "Practical Input Optimization for Aircraft Parameter Estimation Experiments", NASA CR-191242, May 1993.
13. Morelli, E. A. and Klein, V., "Optimal Input Design for Aircraft Parameter Estimation Using Dynamic Programming Principles", AIAA paper 90-2801, AIAA Atmospheric Flight Mechanics Conference, August 1990.
14. Morelli, E.A., "Flight Test Validation of Optimal Input Design using Pilot Implementation", *in* Proceedings of the 10th IFAC Symposium on System Identification, Danish Automation Society, Vol. 3, July 1994, pp. 43-8.
15. Morelli, E.A., "Optimal Input Design for Closed Loop Modeling at High Angles of Attack", AIAA paper 96-3418, AIAA Atmospheric Flight Mechanics Conference, July 1996.

16. Morelli, E.A. "Flight Test Validation of Optimal Input Design and Comparison to Conventional Inputs", AIAA paper 97-3711, AIAA Atmospheric Flight Mechanics Conference, August 1997.

17. van der Linden, C.A.A.M., Mulder, J.A., and Sridhar, J.K., "Recent Developments in Aircraft Parameter Identification at Delft University of Technology - Optimal Input Design", *Aerospace Vehicle Dynamics and Control*, Clarendon Press, Oxford, 1994, pp. 259-84.

18. Maine, R.E. and Iliff, K.W., "Application of Parameter Estimation to Aircraft Stability and Control - The Output-Error Approach", NASA RP 1168, June 1986.

19. Morelli, E.A. and Klein, V., "Determining the Accuracy of Maximum Likelihood Parameter Estimates with Colored Residuals", NASA CR 194893, March 1994.

20. Kempel, R. "F-18 High Alpha Research Vehicle Description", Internal Document, NASA Dryden Flight Research Facility, Edwards, CA.

21. Klein, V., and Morgan, D.R. "Estimation of Bias Errors in Measured Airplane Responses using Maximum Likelihood Method", NASA TM-89059, January 1987.

22. Messina, M.D., et al., "Simulation Model of the F/A-18 High Angle-of-Attack Research Vehicle Utilized for the Design of Advanced Control Laws", NASA TM-110216, May 1996.

23. Morelli, E.A., "Estimating Noise Characteristics from Flight Test Data using Optimal Fourier Smoothing", Journal of Aircraft, *32*, 4, July-August 1995, pp. 689-695.

24. Klein, V. "Aircraft Parameter Estimation in Frequency Domain", AIAA paper 78-1344, AIAA Atmospheric Flight Mechanics Conference, August 1978.

25. Morelli, E.A. and Klein, V., "Accuracy of Aerodynamic Model Parameters Estimated from Flight Test Data", Journal of Guidance, Control, and Dynamics, *20*, 1, January-February 1997, pp. 74-80.

26. Morelli, E.A. "In-Flight System Identification", AIAA paper 98-4261, AIAA Atmospheric Flight Mechanics Conference, August 1998.

Table 1 Maximum Likelihood Results
for Lateral-Directional OBES Maneuvers
F-18 HARV, 0.6 / 25K, $\alpha = 5°$

Parameter	*a priori* Estimate	3-2-1-1 Estimate ±Std. Error	Optimal Estimate ±Std. Error	Std. Error Percent Change
Y_β	–0.1316	–0.0970 ±0.0013	–0.0859 ±0.0012	–7.2
Y_{δ_r}	0.0285	0.0304 ±0.0009	0.0327 ±0.0008	–14.1
Y_{δ_a}	0.0053	0	0	†
L_β	–11.56	–11.376 ±0.048	–10.764 ±0.037	–22.8
L_p	–1.592	–1.8120 ±0.0070	–1.7998 ±0.0055	–21.1
L_r	0.5462	0.3396 ±0.0224	0.1727 ±0.0200	–10.4
L_{δ_r}	1.910	2.3074 ±0.0398	1.8768 ±0.0316	–20.7
L_{δ_a}	–15.81	–19.480 ±0.0623	–17.470 ±0.0441	–29.3
N_β	2.139	1.2807 ±0.0039	1.3120 ±0.0028	–27.9
N_p	–0.0085	0	0	†
N_r	–0.0940	–0.1027 ±0.0021	–0.0436 ±0.0019	–11.7
N_{δ_r}	–1.223	–1.3924 ±0.0056	–1.3450 ±0.0043	–23.5
N_{δ_a}	0.2444	0.1738 ±0.0038	0.2383 ±0.0028	–26.6

† = parameter dropped in model structure determination

Table 2 Maximum Likelihood Results
for Longitudinal OBES Maneuvers
F-18 HARV, 0.6 / 25K, $\alpha = 5°$

Parameter	*a priori* Estimate	3-2-1-1 Estimate ±Std. Error	Optimal Estimate ±Std. Error	Std. Error Percent Change
Z_α	–0.5832	–0.5940 ±0.0126	–0.6050 ±0.0047	–62.8
Z_q	0.0	0	0	†
Z_{δ_s}	–0.1093	–0.0378 ±0.0063	–0.0789 ±0.0032	–49.3
M_α	–2.2600	–4.543 ±0.080	–2.195 ±0.012	–85.1
M_q	–0.2927	–4.746 ±0.109	–1.341 ±0.014	–86.8
M_{δ_s}	–6.0380	–5.482 ±0.104	–4.597 ±0.024	–76.4

† = parameter dropped in model structure determination

Table 3 Maximum Likelihood Results
for Longitudinal Pilot Maneuvers
F-18 HARV, 0.4 / 25K, $\alpha = 20°$

Parameter	Compound Doublet Std. Error	Optimal Std. Error	Std. Error Percent Change
Z_α	0.0069	0.0027	–61.4
Z_q	0.0044	0.0028	–35.1
Z_{δ_s}	0.0038	0.0031	–17.0
M_α	0.0114	0.0033	–70.6
M_q	0.0086	0.0039	–54.0
M_{δ_s}	0.0094	0.0052	–45.2

Table 4 Maximum Likelihood Results
for Lateral-Directional Closed Loop OBES Maneuvers
F-18 HARV, 0.25 / 24K, $\alpha = 60°$

Parameter	*A Priori* Value	Optimal Estimate	Optimal Std. Error
Y_β	–0.062	–0.044	0.0018
Y_p	0.002	0	†
Y_r	–1.059	–0.989	0.001
Y_{η_r}	0.336	–0.00252	0.00012
Y_{η_a}	–0.796	–0.1908	0.0034
L_β	–1.705	–2.103	0.070
L_p	–0.730	–0.643	0.024
L_r	0.309	0.684	0.048
L_ϕ	–0.005	0	†
L_{η_r}	–3.022	–0.0387	0.0044
L_{η_a}	26.99	7.293	0.146
N_β	2.435	4.066	0.040
N_p	0.122	0.389	0.027
N_r	–1.293	–1.334	0.032
N_ϕ	0.083	0	†
N_{η_r}	17.88	0.176	0.004
N_{η_a}	–4.876	–3.579	0.103
τ_r	0	0.037	*
τ_a	0	0.038	*

† = parameter dropped in model structure determination

* = fixed parameter

Table 5 Maximum Likelihood Results
for Lateral-Directional Closed Loop Pilot Maneuvers
F-18 HARV, 0.28 / 24K, $\alpha = 30°$

Parameter	*A Priori* Value	Optimal Estimate	Optimal Std. Error
Y_β	–0.043	–0.102	0.004
Y_p	0.018	0.044	0.002
Y_r	–1.015	–0.918	0.004
Y_{η_r}	0.142	–0.00080	0.00015
Y_{η_a}	–1.121	–0.2818	0.0084
L_β	–2.800	–7.708	0.296
L_p	–1.669	–2.519	0.0817
L_r	–0.101	0	†
L_ϕ	0.080	0.895	0.079
L_{η_r}	–20.36	–0.3415	0.0096
L_{η_a}	81.16	11.66	0.42
N_β	1.638	6.331	0.124
N_p	0.142	0	†
N_r	–1.703	–2.600	0.066
N_ϕ	0.140	–0.515	0.039
N_{η_r}	13.18	0.2104	0.0057
N_{η_a}	–7.183	1.671	0.182
τ_r	0	0.046	*
τ_a	0	0.022	*

† = parameter dropped in model structure determination

* = fixed parameter

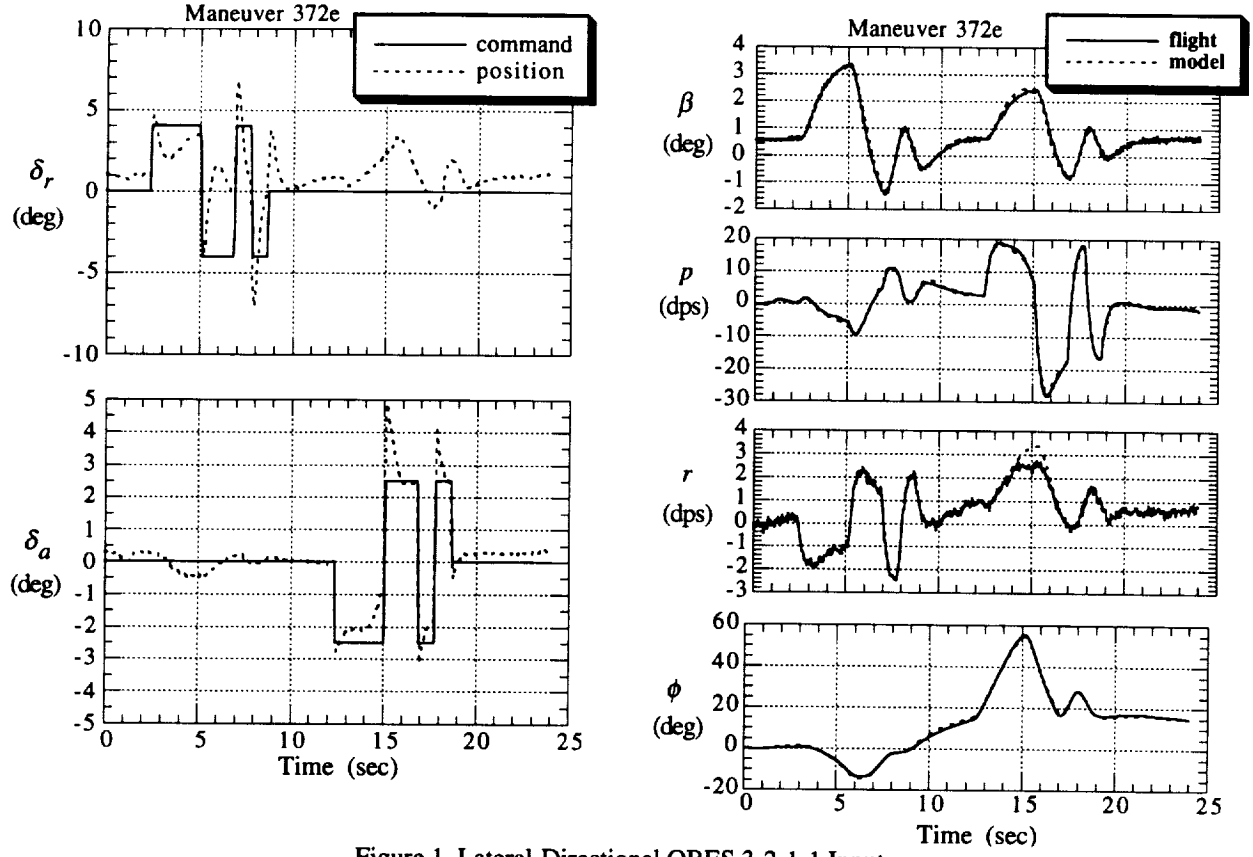

Figure 1 Lateral-Directional OBES 3-2-1-1 Input
F-18 HARV, 0.6 / 25K, a = 5°

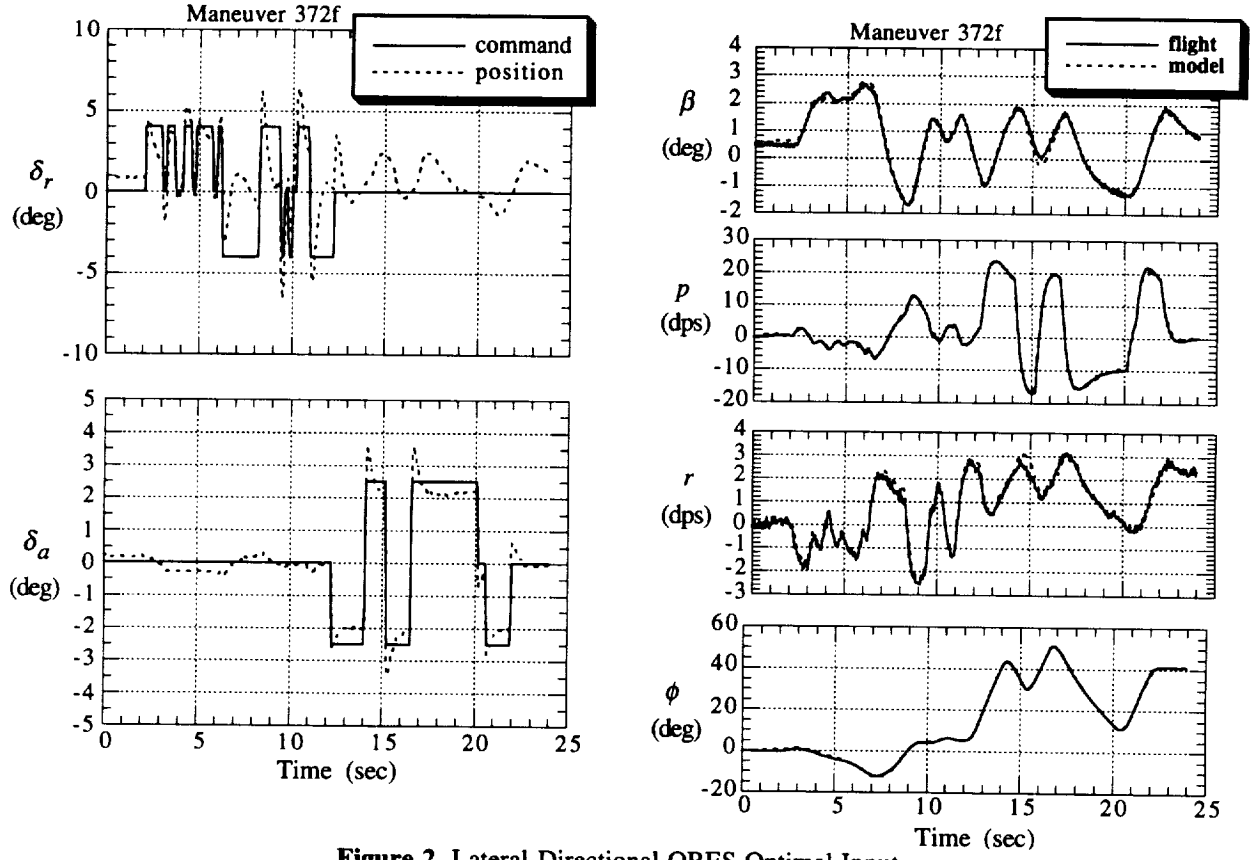

Figure 2 Lateral-Directional OBES Optimal Input
F-18 HARV, 0.6 / 25K, $\alpha = 5°$

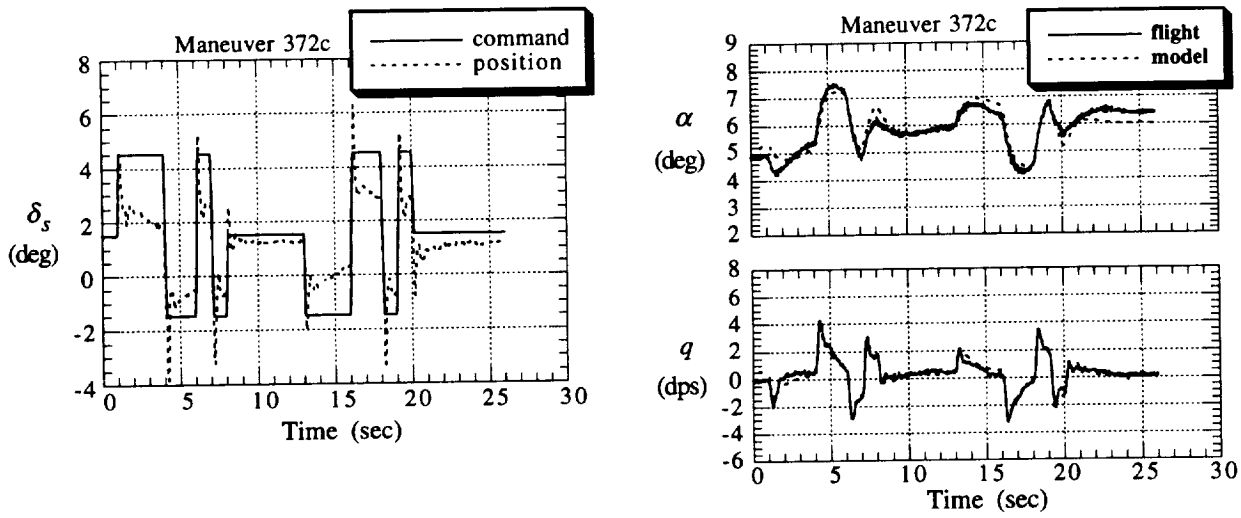

Figure 3 Longitudinal OBES 3-2-1-1 Input
F-18 HARV, 0.6 / 25K, $\alpha = 5°$

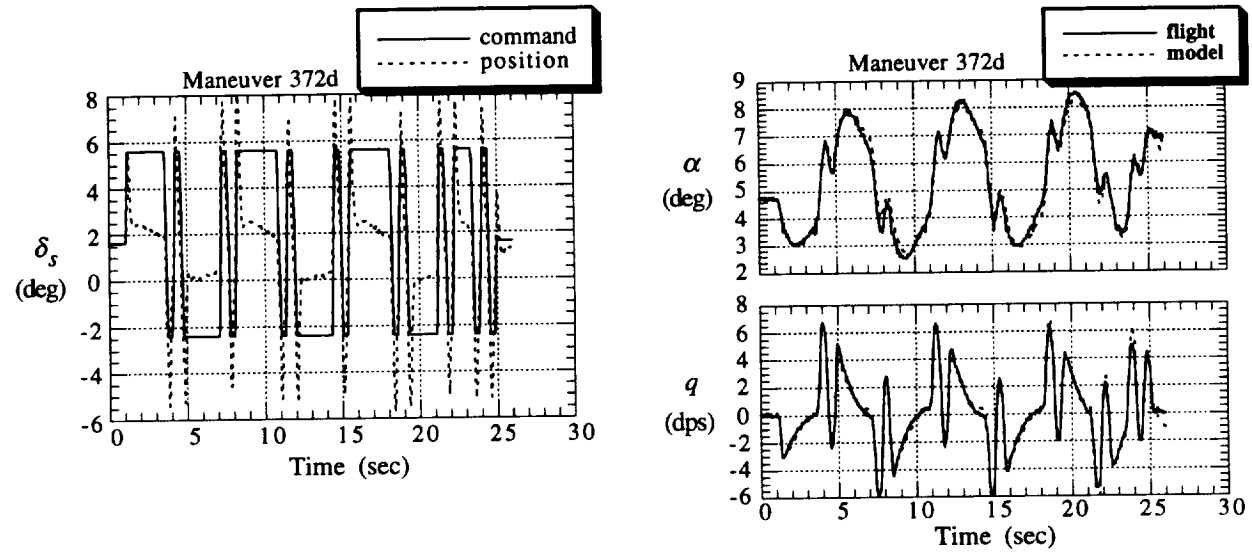

Figure 4 Longitudinal OBES Optimal Input
F-18 HARV, 0.6 / 25K, $\alpha = 5°$

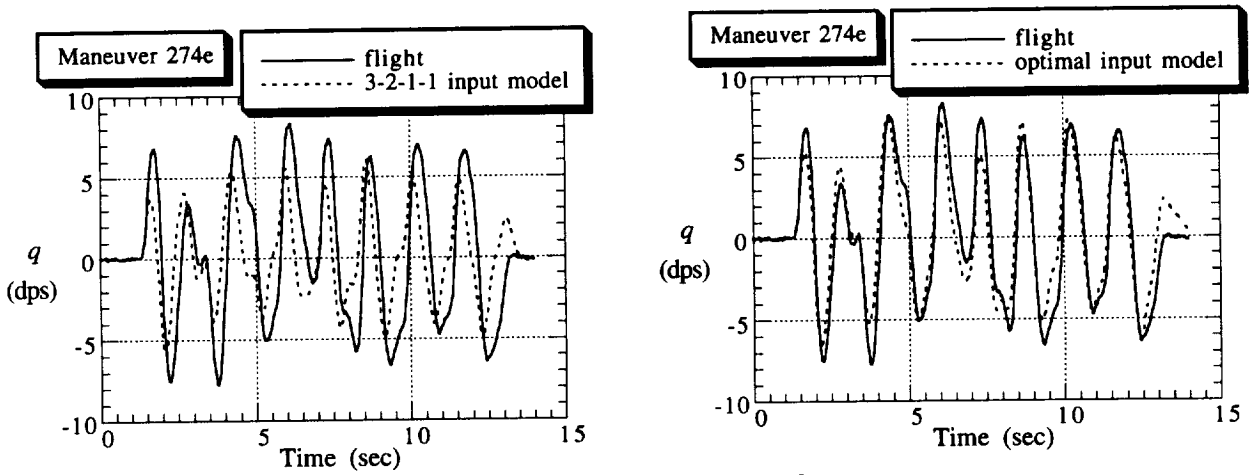

Figure 5 Longitudinal Prediction Case
F-18 HARV, 0.6 / 25K, $\alpha = 5°$

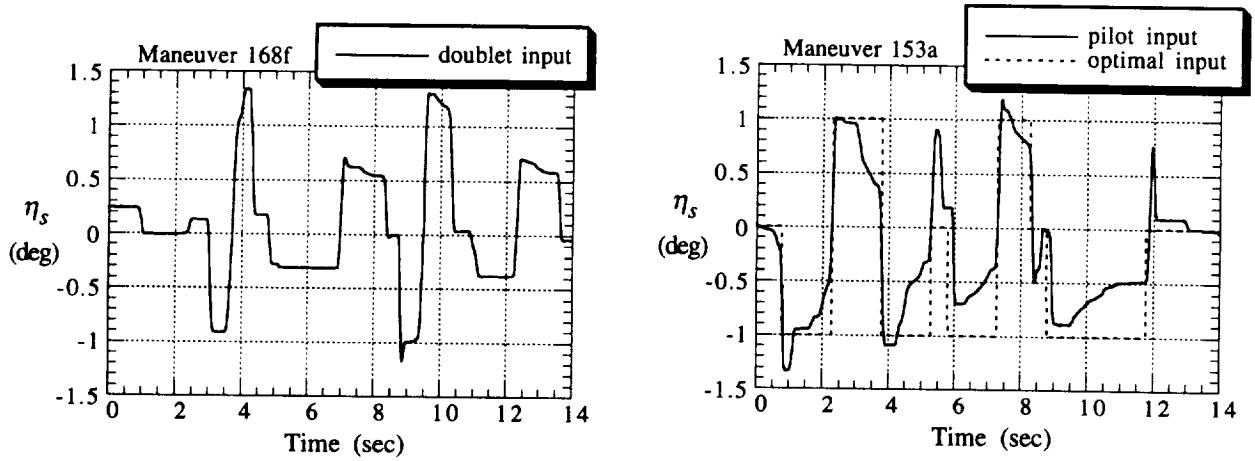

Figure 6 Longitudinal Pilot Inputs
F-18 HARV, 0.4 / 25K, $\alpha = 20°$

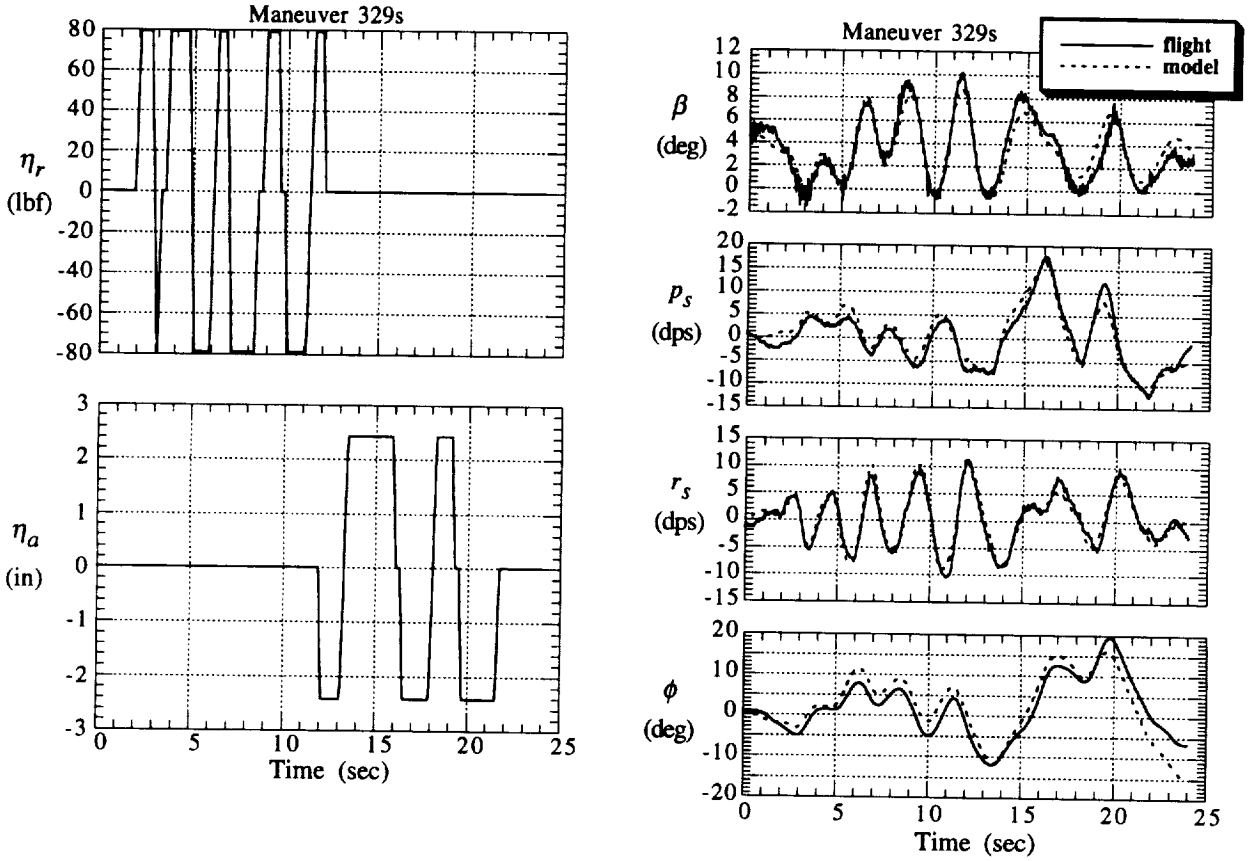

Figure 7 Lateral-Directional Closed Loop OBES Optimal Input
F-18 HARV, 0.25 / 24K, $\alpha = 60°$, TV Mode

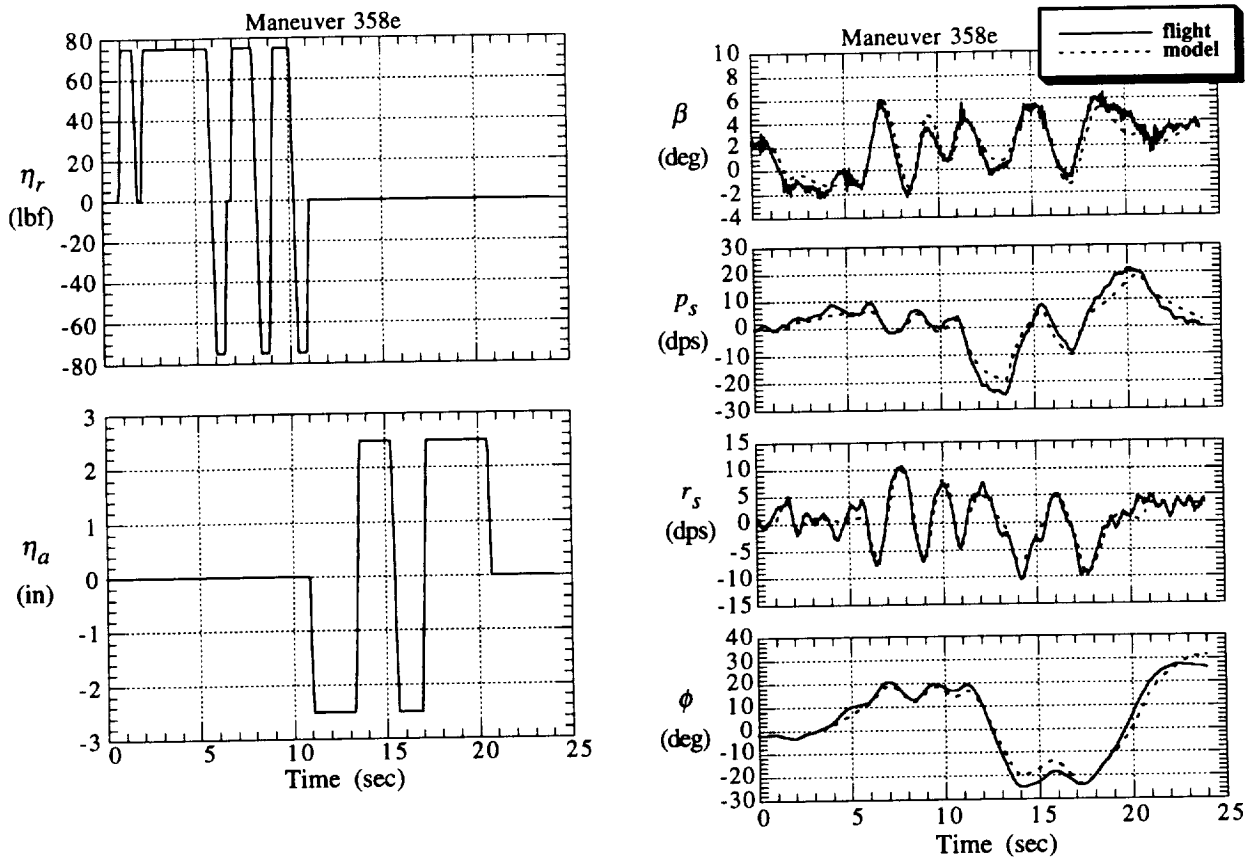

Figure 8 Lateral-Directional Closed Loop OBES Prediction Case
F-18 HARV, 0.25 / 24K, $\alpha = 60°$, TV Mode

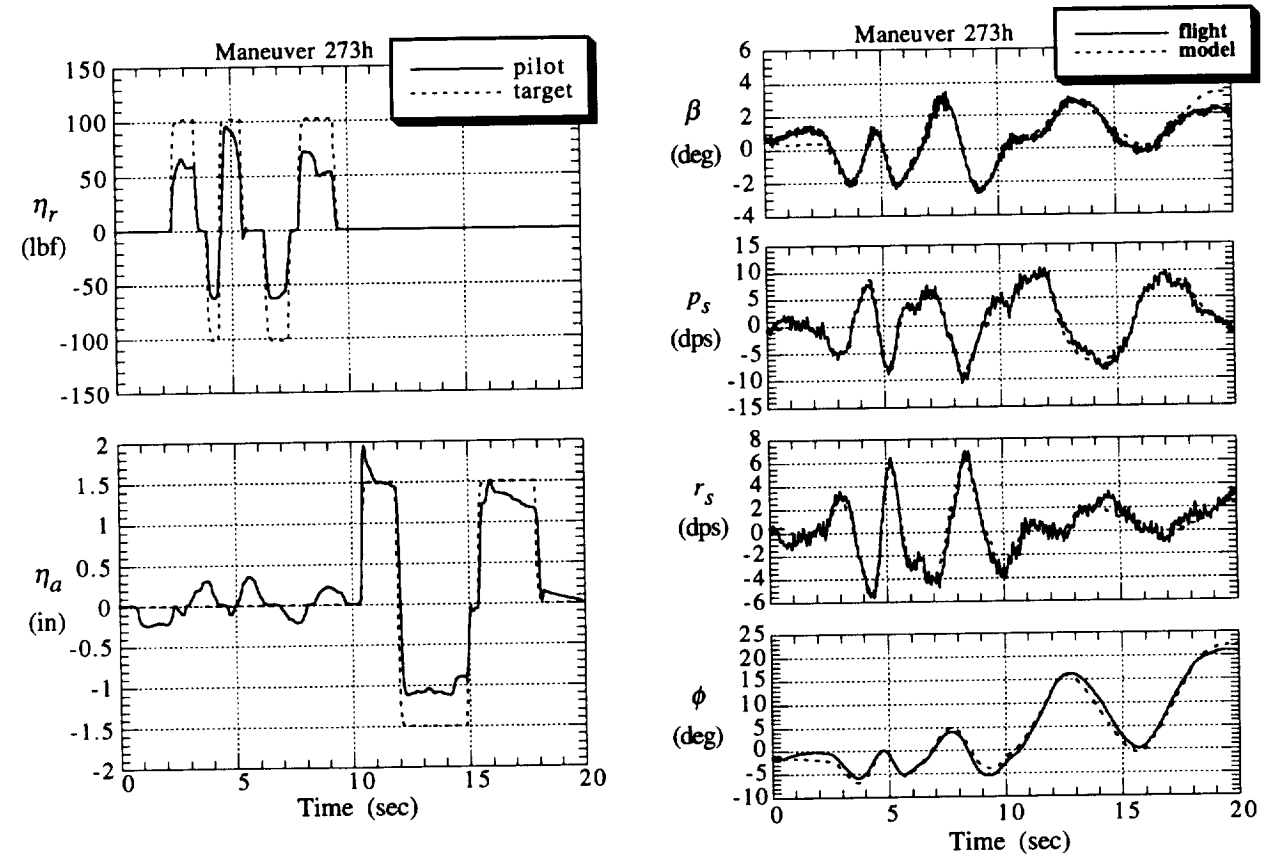

Figure 9 Lateral-Directional Closed Loop Pilot Optimal Input
F-18 HARV, 0.28 / 24K, $\alpha = 30°$, TV Mode